Experimental Study of Model-Free Vibration Control Based on a Virtual Controlled Object Considering Parameter Uncertainty of Actuator

Ansei Yonezawa#1, Heisei Yonezawa#2, Itsuro Kajiwara#3

#1
Graduate Student
Division of Human Mechanical Systems and Design, Hokkaido University
N13, W8, Kita-ku, Sapporo 060-8628, Japan
Phone +81-90-2893-3160
E-mail: ansei316@eis.hokudai.ac.jp

#2
Assistant Professor
Division of Mechanical and Aerospace Engineering, Hokkaido University
N13, W8, Kita-ku, Sapporo 060-8628, Japan
Phone +81-80-4039-9406
E-mail: heisei620@gmail.com

#3 (Corresponding author)
Professor
Division of Mechanical and Aerospace Engineering, Hokkaido University
N13, W8, Kita-ku, Sapporo 060-8628, Japan
Phone +81-11-706-6390, Fax. +81-11-706-6390
E-mail: ikajiwara@eng.hokudai.ac.jp

Abstract

This study experimentally verifies robustness of a model-free vibration controller based on a virtual controlled object (VCO) considering parametric uncertainty of actuator. A proof-mass actuator, which can be modeled as a single-degree-of-freedom (SDOF) system, is used. A VCO, which is defined as an SDOF structure, is introduced between a real controlled object and the actuator model. The parameters of the VCO are determined so as to achieve model-free vibration control. A state equation to derive the model-free controller is constructed using the two-degree-of-freedom (2DOF) structure composed of the actuator model and the VCO. The parametric uncertainty of the actuator is quantitatively characterized in the 2DOF structure. The mixed H_2/H_∞ control theory is used to design a model-free controller. The vibration suppression performance and robustness to the actuator uncertainty of the proposed method are validated by experiments. Simulation studies are also conducted to enhance the validity of the experimental results. As a result, the proposed damping method exhibits good damping performance and strong robustness to the actuator uncertainty and characteristic changes in controlled object.

Keywords

Active vibration control, model-free control, virtual controlled object, proof-mass actuator, parametric uncertainty, mixed H_2/H_∞ control

1. Introduction

Vibration suppression is necessary for downsizing, reducing the weight, and improving the performance of mechanical systems. Especially, active vibration control has been widely examined because of its good vibration reduction performance [1–3]. For example, an active vibration control method for an automotive drive system with backlash has been investigated [4–6]. In general, mathematical models of controlled objects are needed to design active vibration control systems. That is, mathematical modeling of controlled objects is needed—specifically, model-based control [7,8]. However, such modeling processes are costly and troublesome for designers. In addition, modeling errors, which always exist in actual systems, adversely affect the systems' performance, or even destabilize closed-loop systems.

Consequently, numerous studies have examined model-free control, which does not require concrete mathematical models of controlled objects [9,10]. These methods are developed for specific mechanical systems. Introducing neural networks [11,12] and employing fuzzy logic [13,14] are typical model-free control approaches. However, many of these approaches have cumbersome and impractical design procedures due to their complexities. Data-driven control is an effective method to construct a control system without using concrete mathematical models of controlled objects [15–17]. Typically, such a technique requires many parameters to be tuned to derive an appropriate controller.

By contrast, a model-free vibration control based on a virtual controlled object (VCO) has been proposed as a simple and implementable model-free vibration suppression system [18–20]. This approach derives an active vibration controller on the basis of an actuator model and a VCO, implying that the accuracy of the actuator model heavily influences the closed-loop stability and

damping performance of the system [21,22]. In general, actuators have parametric uncertainties that originate from their aging and their individual differences. Studies have examined VCO-based model-free vibration control that considers the actuator uncertainty [21,22]. Nevertheless, these methods have several problems, such as conservativeness of the damping performance [21] and a chattering phenomenon [22], that diminish their practical applicability. On the other hand, the model-free mixed H_2/H_∞ vibration control considering actuator uncertainty can overcome the problems which deteriorate the practicability [23]. However, the basic properties of this damping scheme such as robustness to the characteristic changes in real controlled object has not been studied.

In this study, robustness of the VCO-based model-free mixed H_2/H_∞ control considering parameter uncertainty of actuator is experimentally validated. A proof-mass actuator is used in the present work because it can be modeled as a single-degree-of-freedom (SDOF) system [18]. First, a VCO, which is defined as an SDOF system, is inserted between an actual controlled object and the SDOF actuator model. Setting appropriate VCO parameters considering frequency transfer characteristic from the actual controlled object to the VCO results in model-free active vibration suppression. A state equation for model-free controller design is derived using the two-degrees-of-freedom (2DOF) system composed of the SDOF actuator and the VCO. Second, parametric uncertainty occurring in the actuator is quantitatively evaluated in the 2DOF system. The mixed H_2/H_∞ control theory is applied for the uncertain 2DOF plant to establish a model-free controller considering the actuator uncertainty. An advantage of the VCO-method is that various model-based control theories can be used to design the controller without controlled object modeling. Moreover, the proposed control technique has strong robustness to the parametric uncertainty of the actuator and good damping performance. Finally, vibration control experiments validate the damping performance and robustness to the actuator uncertainty and characteristic changes in

controlled object of the proposed control scheme. An aluminum plate structure and the aluminum plate with a 1.37 kg weight on it are used for the controlled objects in the experiments. As a result, the proposed control scheme realizes good vibration suppression for both controlled objects despite the actuator uncertainty.

Compared with the previous study exploring the design method of the VCO-based model-free control [19], this study is devoted to improving the robustness of the model-free vibration control based on the VCO to the parametric uncertainty of the actuator, whereas the previous study [19] focuses on the controller tuning issue for the VCO-based model-free control. The controller proposed in the previous work [19] was designed based on the simple linear quadratic regulator theory and did not consider the parametric uncertainty of the actuator. Moreover, the previous study [19] lacks the robustness verification to the actuator uncertainty. However, unlike the previous work [19], this study proposes a novel VCO-based model-free controller design using the mixed H_2/H_∞ synthesis with consideration of the actuator uncertainty. The robustness to the parametric error of the actuator is experimentally validated. The actuators in real mechanical systems often have parametric uncertainties that originate from their aging and their individual differences, significantly affecting the system performance. Therefore, this study further thrusts the VCO-based vibration control forward to the practical implementations.

One of the representative virtues of the technique proposed in this study is that the proposed method is robust to uncertainties of both actual controlled objects and parameters of actuator. Hence, the proposed method can be employed for various vibration suppression problems of mechanical systems that require high reliability or have uncertainties. This technique is expected to be applied to a variety of mechanical systems, such as machine tools, automotive systems (e.g.,

engine mount system), aerospace structures, and mechanical products with large individual differences.

The main limitation of the proposed method is that the actuator must be mounted directly to the place where vibrations should be reduced. Due to various limitations such as lack of space, the actuator is not always attachable to every mechanical structure freely.

However, if the actuator can be implemented directly to the damping point, the proposed method has significant advantages over conventional passive vibration mitigation methods and model-based active control approaches. To name a few, the proposed method is expected to replace a passive damping using multiple tuned mass dampers for machine tool chatter [24] and a model-based active vibration control for floor structure via inertial actuators [25]. Compared with the passive vibration mitigation, which often requires multiple damping equipment, active vibration control methodology is effective in wide frequency range of vibrations via simpler system configuration. Moreover, compared with the traditional model-based control, the proposed method has much simpler design process because of its model-free nature.

2. Basic concepts of VCO-based model-free control

2.1. Actuator

The actuator used in this study is shown in Figure 1. It is an electromagnetic proof-mass actuator. Such an actuator can be modeled as an SDOF system because of its mechanical properties [18]. Hereafter, m_0, c_0, k_0 denote the mass, damping, and stiffness of the actuator, respectively. In this

study, $m_0 = 0.2013$ kg, $c_0 = 1.186$ Ns/m, and $k_0 = 3518$ N/m [18]. These parameter values are obtained via the system identification. x_0 represents the displacement of the point mass of the actuator.

2.2. VCO

Inserting an SDOF VCO between the actuator and an actual controlled object achieves model-free control. The actual mechanical system is described in Figure 2(a). The control input u generated by the actuator suppresses vibration x_1 at the actuator mounting position of the actual controlled object. Figure 2(b) shows the model used for controller design. The VCO is introduced between the actuator and the actual controlled object shown in Figure 2(a). m_v, c_v, k_v denote the mass, damping, and stiffness of the VCO, respectively, and x_v does the displacement of the point mass of the VCO. The fundamental principle of the VCO-based model-free control is that the vibration of the actual controlled object, x_1, is damped indirectly by suppressing that of the VCO, x_v [18].

The equations of motion of the actuator and the VCO in Figure 2(b) are

$$m_0\ddot{x}_0 + c_0(\dot{x}_0 - \dot{x}_v) + k_0(x_0 - x_v) = u \tag{1}$$

$$m_v\ddot{x}_v + c_v(\dot{x}_v - \dot{x}_1) + k_v(x_v - x_1) + c_0(\dot{x}_v - \dot{x}_0) + k_0(x_v - x_0) = -u \tag{2}$$

Laplace transforming equations (1) and (2) yields equation (3). s denotes the Laplace variable. The Laplace transformed functions are represented as capital letters. T_{xvx1} is the transfer property from x_1 to x_v.

$$T_{xvx1} = \frac{X_v(s)}{X_1(s)} = \frac{(m_0s^2 + c_0s + k_0)(c_vs + k_v)}{\{m_vs^2 + (c_0 + c_v)s + (k_0 + k_v)\}(m_0s^2 + c_0s + k_0) - (c_0s + k_0)^2} \tag{3}$$

The parameters of the VCO—specifically, m_v, c_v, and k_v—are determined so as to achieve model-free vibration control. The inequalities (4) and (5) have been proposed in a previous study to design such an appropriate VCO [18]:

$$\left[\left\{\frac{\left(\Omega_{upper}\right)^2}{k_0}-\frac{1}{m_0}\right\}k_v+\left(\Omega_{upper}\right)^2\right]\frac{1}{m_v}>\left(\frac{\left(\Omega_{upper}\right)^2}{k_0}-\frac{1}{m_0}\right)\left(\Omega_{upper}\right)^2 \tag{4}$$

$$\left[\left\{\frac{(\Omega_{lower})^2}{k_0}-\frac{1}{m_0}\right\}k_v+(\Omega_{lower})^2\right]\frac{1}{m_v}>\left(\frac{(\Omega_{lower})^2}{k_0}-\frac{1}{m_0}\right)(\Omega_{lower})^2 \tag{5}$$

where Ω_{upper} and Ω_{lower} are the upper and the lower bound frequencies, respectively, of a controlled frequency band satisfying $\Omega_{upper} > \Omega_{lower} \geq \sqrt{k_0/m_0}$. In this study, the controlled frequency band is 50–1000 Hz.

When conditions (4) and (5) are satisfied, $T_{xvx1} \approx 1$ is realized in the controlled frequency band, implying that $x_1 \approx x_v$ holds and that indirect vibration suppression is achieved [18]. This study uses $m_v = 1.0 \times 10^{-5}$ kg, $c_v = 0.0$ Ns/m, and $k_v = 7.0 \times 10^5$ N/m [18]. Figure 3 shows the Bode plot of T_{xvx1}, demonstrating that $T_{xvx1} \approx 1$ (i.e., $x_1 \approx x_v$) is achieved in the controlled frequency band.

It should be noted that the purpose of this study is to suppress the vibration at the actuator mounting position on the actual controlled object. This is because the actuator and the damping point (the position of the sensor to get the measured output) must be collocated to achieve the VCO-based model-free vibration control. Closed-loop control is performed by feeding the vibration of the VCO back as the measured output. Nevertheless, the VCO does not exist in the real mechanical system. Hence, vibration x_1 of the actual controlled object, which is almost equal to x_v because $T_{xvx1} \approx 1$, is used as the measured output. In particular, x_1 at the actuator mounting location is measured by a sensor and suppressed when the actual controlled object is a continuous structure [19].

2.3. State equation to design a VCO-based model-free controller

In equations (1) and (2), disturbance w is defined as

$$w = c_v\dot{x}_1 + k_v x_1 \tag{6}$$

Equations (1), (2), and (6) yield the state equation for model-free controller design as

$$\dot{x}_{va} = A_{va}x_{va} + B_{va1}w + B_{va2}u \tag{7}$$

$$x_{va} = [x_v \quad x_0 \quad \dot{x}_v \quad \dot{x}_0]^T \tag{8}$$

$$A_{va} = \begin{bmatrix} 0 & 0 & 1 & 0 \\ 0 & 0 & 0 & 1 \\ -\dfrac{k_0 + k_v}{m_v} & \dfrac{k_0}{m_v} & -\dfrac{c_0 + c_v}{m_v} & \dfrac{c_0}{m_v} \\ \dfrac{k_0}{m_0} & -\dfrac{k_0}{m_0} & \dfrac{c_0}{m_0} & -\dfrac{c_0}{m_0} \end{bmatrix} \tag{9}$$

$$B_{va1} = \begin{bmatrix} 0 & 0 & \dfrac{1}{m_v} & 0 \end{bmatrix}^T \tag{10}$$

$$B_{va2} = \begin{bmatrix} 0 & 0 & -\dfrac{1}{m_v} & \dfrac{1}{m_0} \end{bmatrix}^T \tag{11}$$

Notably, equation (7) is a simple and low-order state equation that does not contain any parameters or models of the actual controlled object. Hence, a model-free vibration controller based on a VCO can be easily derived by applying familiar model-based control theories to equation (7).

3. Model-free controller with robustness to parametric uncertainty of an actuator

The accuracy of the actuator parameter is critical to the vibration suppression performance and closed-loop stability because equation (7) includes the actuator parameters [21,22]. However, actuators always have parametric uncertainties due to modeling errors, individual differences, and aging. Consequently, the VCO-based controller design should take such parametric uncertainties into account. This study considers the uncertainties in an actuator's damping and stiffness—c_0 and k_0—because their exact values are generally more difficult to obtain than the actuator's mass, m_0.

3.1. Characterization of actuator's parametric uncertainty

The uncertain damping c_{0m} and stiffness k_{0m} of the actuator can be modelled as:

$$c_{0m} = c_{0n} + \Delta_c c_e \tag{12}$$

$$k_{0m} = k_{0n} + \Delta_k k_e \tag{13}$$

Here, the nominal values are indicated by the subscript $0n$. The maximum errors occurring in the actuator damping and stiffness are denoted as c_e and k_e, respectively. Δ_c and Δ_k are the fluctuations satisfying $|\Delta_{c,k}| \leq 1$. The nominal parameters and the maximum errors are assumed to be known.

Substituting c_{0m} and k_{0m} for c_0 and k_0 in equations (1) and (2) yields equations (14)–(20).

$$\tilde{P}(s) = \frac{s^2 X_v}{U} = \frac{P(s)}{1 + \Delta W(s)} \tag{14}$$

$$P(s) \tag{15}$$

$$= \frac{-m_0 s^4}{m_0 m_v s^4 + (m_0 + m_v)c_{0n}s^3 + \{(m_0 + m_v)k_{0n} + m_0 k_v\}s^2 + c_{0n}k_v s + k_{0n}k_v}$$

$$W(s) = \begin{bmatrix} W_1(s) \\ W_2(s) \end{bmatrix} = \frac{1}{W_{den}(s)} \begin{bmatrix} W_{1num}(s) \\ W_{2num}(s) \end{bmatrix} \tag{16}$$

$$W_{den}(s) = m_0 m_v s^4 + (m_0 + m_v)c_{0n}s^3 + \{(m_0 + m_v)k_{0n} + m_0 k_v\}s^2 + c_{0n}k_v s + k_{0n}k_v \tag{17}$$

$$W_{1num}(s) = (m_0 + m_v)c_e s^3 + k_v c_e s \tag{18}$$

$$W_{2num}(s) = (m_0 + m_v)k_e s^2 + k_v k_e \tag{19}$$

$$\Delta = [\Delta_c \quad \Delta_k] \tag{20}$$

$\tilde{P}(s)$ is the transfer function from control input u to measured output $\ddot{x}_v$ when the actuator has the parametric uncertainties. $P(s)$ represents the nominal transfer function from u to $\ddot{x}_v$. Equation (14) implies that the uncertain transfer function $\tilde{P}(s)$ can be modelled as the plant set of $P(s)$ with the feedback-type fluctuations as shown in Figure 4 [21,26].

3.2. Model-free mixed H_2/H_∞ controller design

For equation (14), the generalized plant G for a robust controller design is constructed as Figure 5 for the evaluation with the small-gain theorem [26]. Equations (21)–(29) show formulations of each property shown in Figure 5; w_d is the disturbance and z_{H2} and $z_{H\infty}$ are the controlled outputs.

$$P: \begin{cases} \dot{x}_P = A_P x_P + B_{P1} w_p + B_{P2} u \\ y = C_P x_P + D_{P1} w_p + D_{P2} u \end{cases} \tag{21}$$

$$y_a = y - w_e \tag{22}$$

$$W_1 : \begin{cases} \dot{x}_{w1} = A_{w1}x_{w1} + B_{w1}y_a \\ z_{w1} = C_{w1}x_{w1} + D_{w1}y_a \end{cases} \tag{23}$$

$$W_2 : \begin{cases} \dot{x}_{w2} = A_{w2}x_{w2} + B_{w2}y_a \\ z_{w2} = C_{w2}x_{w2} + D_{w2}y_a \end{cases} \tag{24}$$

$$I : \begin{cases} \dot{x}_I = A_I x_I + B_I y_a \\ y_{vl} = C_I x_I + D_I y_a \end{cases} \tag{25}$$

$$z_1 = Q y_{vl} \tag{26}$$

$$z_u = Ru \tag{27}$$

$$z_{H2} = z_1 \tag{28}$$

$$z_{H\infty} = [z_u \quad z_{w1} \quad z_{w2}]^T \tag{29}$$

Equation (21) is the state-space realization of equation (15) and is the state equation of the nominal actuator and the VCO. y is the acceleration $\ddot{x}_v$ of the VCO when the actuator is nominal. Equations (23) and (24) are the state-space realizations of $W_1(s)$ and $W_2(s)$ in equation (16), respectively. Equation (25) is the state-space realization of the approximate integrator shown in equation (30). In equation (30), δ is a small positive value. Q and R in equations (26) and (27) are constant weights. In this study, $\delta = 1.0 \times 10^{-7}$, $Q = 1.0 \times 10^{0}$, and $R = 1.2 \times 10^{1}$. They were empirically determined by actually conducting the vibration control experiments for Structure 1 described in Chapter 4 when the actuator is nominal.

$$I(s) = \frac{1}{s + \delta} \tag{30}$$

The controller K is derived on the basis of the mixed H_2/H_∞ control theory [27,28] for both compensating the parametric uncertainty of the actuator and suppressing the vibration. In particular, for the closed-loop system in Figure 5, K is designed so as to minimize the H_2 norm of T_{zH2wd} (the closed-loop transfer function from w_d to z_{H2}) under the H_∞ norm constraint of $T_{zH\infty wd}$ (the

closed-loop transfer function from w_d to $z_{H\infty}$). The controller was numerically derived using the Control System Toolbox and Robust Control Toolbox of MATLAB.

4. Experimental study

4.1. Experimental setup

The effectiveness of the proposed control scheme was verified via vibration control experiments. Figure 6 shows the controlled objects used in this study. Hereafter, the structure described in Figure 6(a) (an aluminum cantilever plate with dimensions 248 mm × 190 mm × 10 mm) is referred to as Structure 1 and that described in Figure 6(b) (Structure 1 with a 1.37 kg weight on it) is referred to as Structure 2. The 1.37kg mass was fixed to the cantilever plate using an adhesive. A load cell was installed at position A to apply an exciting force with a shaker and to measure the force. The actuator mounted at position B provided the control input. The measured output was obtained via an accelerometer attached at position C on the back of the cantilever plate at the actuator mounting position. Figure 7(a) shows the closed-loop system for the experiments. The signal generator applied a 1–1000 Hz linear sweep sinusoidal signal as an excitation disturbance. The measured output obtained by the accelerometer was input into the digital signal processor (DSP). The DSP calculated the control input command value. The command value passed through an analog low-pass filter to prevent spillover and was then amplified by the current amplifier to drive the actuator. A spectrum analyzer measured the frequency response from the disturbance (force obtained from the load cell) to the measured output (acceleration obtained from the sensor). That is, the damping

performance was evaluated via the acceleration of the controlled object. The controlled frequency band was 50–1000 Hz. The experimental setup is shown in Figure 7(b).

It is difficult to use multiple actuators with various parameters to evaluate robustness to the actuator uncertainty in the actual experiments. Therefore, the parameters of the actuator model for controller design (c_{0n}, k_{0n}) were fluctuated from the values which are the parameters of the actuator used for the experiments (c_0, k_0). Designing controllers using such actuator model, the situation where parameter errors occurred was created equivalently for the unique actuator employed in the experiment [21,22]. The error range to be compensated was $\pm 50\%$.

4.2. Results

Table 1 lists main experimental results for Structure 1 [23], and Table 2 does those for Structure 2. ErC and ErK represent that the damping and the stiffness of the actuator parameters employed in the experiment had errors of ErC [%] and ErK [%] with respect to the damping and the stiffness of the actuator employed for controller design, respectively. Figures 8 and 9 show typical frequency responses from the disturbance to the measured output obtained by experiments with Structures 1 and 2, respectively. The black and magenta lines in each graph are the frequency response without control and the closed-loop frequency response with control, respectively.

Table 1. Results of vibration control experiment with Structure 1

Parameters of actuator		Vibration reduction amount [dB]	
ErC [%]	ErK [%]	115 Hz peak	257 Hz peak
0	0	−14.7	−13.7
50	50	−13.9	−13.0
50	−50	−14.6	−13.8
−50	50	−14.7	−11.6
−50	−50	−14.5	−11.4
19.62	−46.65	−14.6	−13.9
−49.00	14.05	−14.7	−13.6
−0.57	−44.06	−14.9	−14.1

Table 2. Results of vibration control experiment with Structure 2

Parameters of actuator		Vibration reduction amount [dB]	
ErC [%]	ErK [%]	98 Hz peak	217 Hz peak
0	0	−6.4	−8.7
50	50	−7.5	−9.4
50	−50	−7.5	−9.6
−50	50	−7.1	−9.4
−50	−50	−7.0	−9.4
19.62	−46.65	−7.2	−9.7
−49.00	14.05	−5.6	−9.6
−0.57	−44.06	−7.1	−9.8

4.3. Comparison with numerical simulation results

The experimental results are compared with the numerical study, enhancing the validity of the experiments. In the simulations, Structure 1 is the controlled object. The plant model for the simulation is obtained by experimental modal analysis [18]. The model-free controller used for the simulations is the same as that used for the experiments. Table 3 lists the simulation results. Figure 10 shows the representative frequency responses obtained by the simulation, where the color has

the same meanings as Figures 8 and 9. Compared with the experimental results, almost the same results are obtained by the simulations.

Table 3. Results of vibration control simulations with Structure 1

Parameters of actuator		Vibration reduction amount [dB]	
ErC [%]	ErK [%]	114 Hz peak	257 Hz peak
0	0	−13.08	−9.48
50	50	−13.41	−9.46
50	−50	−12.43	−8.85
−50	50	−12.97	−9.13
−50	−50	−12.51	−8.94

4.4. Discussion

The results in Tables 1–3 and Figures 8–10 indicate that the proposed controller achieved good damping performance for major peaks without destabilization. Notably, these results were obtained using actuators with parametric uncertainty. These results are attributed to the VCO-based model-free H_2/H_∞ controller design with the evaluation of the parametric errors of the actuator. In particular, the vibration suppression performance is achieved from the point of view of the H_2 norm, and the robustness to the actuator uncertainty is guaranteed in terms of the H_∞ norm. Such design method enables to simultaneously achieve both good vibration suppression performance and strong robustness to the uncertainty. Consequently, the proposed controller performed very well and exhibits strong robustness to the parametric uncertainty of the actuator.

This study employs two controlled objects—Structures 1 and 2—whose characteristics differ from each other. However, although the controller is tuned for Structure 1, the controller reduced the vibrations occurring in both Structures 1 and 2. That is, the same controller suppressed vibrations occurring in different structures, implying that the proposed controller has robustness

not only to the parametric uncertainty of the actuator but also to the uncertainties of the controlled objects. Such robustness to the uncertainties of controlled objects originates from the fact that the proposed controller is designed using the VCO instead of the actual controlled object [19]; that is, robustness is attributable to the controller being model-free. Actual mechanical systems have many uncertainties, including parametric uncertainty of the actuator and characteristic changes of the controlled object. Therefore, the proposed control method is well suited to practical vibration control problems in actual plants in terms of its robustness to the uncertainties.

The proposed control technique can be employed only when both the actuator and the sensor for obtaining the measured output can be directly attached to the point to be damped. This limitation occurs because the VCO-based model-free vibration control can be achieved only when the actuator and the sensor are collocated at the damping point. However, the actuator may not always be attachable at the damping point of an actual mechanical structure because of various limitations, such as a lack of space. If this limitation can be overcome, the versatility of the VCO-based model-free vibration control will be further improved.

5. Conclusion

This study experimentally evaluates the damping performance and robustness of the VCO-based model-free mixed H_2/H_∞ vibration controller. The VCO is introduced between the actuator model and an actual controlled object, yielding the 2DOF plant for model-free controller design. The 2DOF plant is composed only of the actuator and VCO. The influence of the parametric uncertainty of the actuator is quantitatively characterized in the 2DOF plant. The VCO-based model-free

controller that can compensate for the effect of the actuator uncertainty is designed using the mixed H_2/H_∞ synthesis. The vibration control experiments and simulations validate the damping performance and robustness to the actuator uncertainty of the proposed method. Moreover, the experiments also reveal that the novel controller has strong robustness not only to the actuator uncertainty but also to the uncertainty in the characteristics of an actual controlled object.

In the future, the proposed method will be applied to practical mechanical vibration problems such as a chatter reduction in a machine tool [24] and a vibration mitigation in a pedestrian structure [25], examining its effectiveness.

Declaration of competing interest

The authors declare no potential conflicts of interest with respect to the research, authorship, and/or publication of this article.

Funding

We thank the Japan Society for the Promotion of Science for their support (Grant no. JP22J11365).

References

1. Wang L, Li J, Yang Y, et al. Active control of low-frequency vibrations in ultra-precision machining with blended infinite and zero stiffness. *Int J Mach Tools Manuf* 2019; 139: 64–74.
2. Wang W, Li Y, Shi J, et al. Vibration Control Method for an Electric City Bus Driven by a Dual Motor Coaxial Series Drive System Based on Model Predictive Control. *IEEE Access* 2018; 6: 41188–41200.
3. Tang J, Cao D, Yu T. Decentralized vibration control of a voice coil motor-based Stewart parallel mechanism: Simulation and experiments. *Proc Inst Mech Eng Part C J Mech Eng Sci* 2019; 233: 132–145.
4. Yonezawa H, Kajiwara I, Sato S, et al. Vibration control of automotive drive system with nonlinear gear backlash. *J Dyn Syst Meas Control Trans ASME* 2019; 141: 121002.
5. Yonezawa H, Kajiwara I, Nishidome C, et al. Active vibration control of automobile drivetrain with backlash considering time-varying long control period. *Proc Inst Mech Eng Part D J Automob Eng* 2021; 235: 773–783.
6. Yonezawa H, Kajiwara I, Nishidome C, et al. Vibration control of automotive drive system with backlash considering control period constraint. *J Adv Mech Des Syst Manuf* 2019; 13: 1–16.
7. Kant M, Parameswaran AP. Modeling of low frequency dynamics of a smart system and its state feedback based active control. *Mech Syst Signal Process* 2018; 99: 774–789.

8. Hao S, Yamashita Y, Kobayashi K. Active Vibration Control of Nonlinear 2DOF Mechanical Systems via IDA-PBC. *IEICE Trans Fundam Electron Commun Comput Sci* 2020; E103A: 1078–1085.
9. Meurers T, Veres SM, Tan ACH. Model-free frequency domain iterative active sound and vibration control. *Control Eng Pract* 2003; 11: 1049–1059.
10. Wei C, Luo J, Dai H, et al. Adaptive model-free constrained control of postcapture flexible spacecraft: a Euler–Lagrange approach. *J Vib Control* 2018; 24: 4885–4903.
11. Yousefi H, Hirvonen M, Handroos H, et al. Application of neural network in suppressing mechanical vibration of a permanent magnet linear motor. *Control Eng Pract* 2008; 16: 787–797.
12. Abdeljaber O, Avci O, Inman DJ. Active vibration control of flexible cantilever plates using piezoelectric materials and artificial neural networks. *J Sound Vib* 2016; 363: 33–53.
13. Bui H-L, Nguyen C-H, Bui V-B, et al. Vibration control of uncertain structures with actuator saturation using hedge-algebras-based fuzzy controller. *J Vib Control* 2017; 23: 1984–2002.
14. Edalath S, Kukreti AR, Cohen K. Enhancement of a tuned mass damper for building structures using fuzzy logic. *Journal of Vibration and Control* 2013; 19: 1763–1772.
15. Rădac M-B, Precup R-E, Petriu EM, et al. Application of IFT and SPSA to servo system control. *IEEE Trans Neural Networks* 2011; 22: 2363–2375.
16. Remes CL, Gomes RB, Flores JV, et al. Virtual Reference Feedback Tuning Applied to DC-DC Converters. *IEEE Trans Ind Electron* 2021; 68: 544–552.

17. Yahagi S, Kajiwara I, Shimozawa T. Slip control during inertia phase of clutch-to-clutch shift using model-free self-tuning proportional-integral-derivative control. *Proc Inst Mech Eng Part D J Automob Eng* 2020; 234: 2279–2290.

18. Yonezawa H, Kajiwara I, Yonezawa A. Experimental verification of model-free active vibration control approach using virtually controlled object. *J Vib Control* 2020; 26: 1656–1667.

19. Yonezawa A, Yonezawa H, Kajiwara I. Parameter tuning technique for a model-free vibration control system based on a virtual controlled object. *Mech Syst Signal Process* 2022; 165: 108313.

20. Yonezawa A, Yonezawa H, Kajiwara I. Vibration control for various structures with time-varying properties via model-free adaptive controller based on virtual controlled object and SPSA. *Mech Syst Signal Process* 2022; 170: 108801.

21. Yonezawa A, Kajiwara I, Yonezawa H. Model-free vibration control based on a virtual controlled object considering actuator uncertainty. *J Vib Control* 2021; 27: 1324–1335.

22. Yonezawa A, Kajiwara I, Yonezawa H. Novel Sliding Mode Vibration Controller With Simple Model-Free Design and Compensation for Actuator's Uncertainty. *IEEE Access* 2021; 9: 4351–4363.

23. Yonezawa A, Yonezawa H, Kajiwara I. Experimental Verification of Model-Free Vibration Control Technique Based on a Virtual Controlled Object Considering Actuator Parameter Uncertainty. In: *Proceedings of the ASME 2021 International Mechanical Engineering Congress and Exposition*. Online: The American Society of Mechanical Engineers, 2021, p. V07AT07A039.

24. Yang Y, Muñoa J, Altintas Y. Optimization of multiple tuned mass dampers to suppress machine tool chatter. *Int J Mach Tools Manuf* 2010; 50: 834–842.

25. Pereira E, Díaz IM, Hudson EJ, et al. Optimal control-based methodology for active vibration control of pedestrian structures. *Eng Struct* 2014; 80: 153–162.

26. Zhou K, Doyle JC, Glover K. *Robust and Optimal Control*. New Jersey: PrenticeHall, 1996.

27. Zhou K, Glover K, Bodenheimer B, et al. Mixed H2 and H∞ Performance Objectives I: Robust Performance Analysis. *IEEE Trans Automat Contr* 1994; 39: 1564–1574.

28. Doyle J, Zhou K, Glover K, et al. Mixed H2 and H∞ Performance Objectives II: Optimal Control. *IEEE Trans Automat Contr* 1994; 39: 1575–1587.

Figure captions list

Figure 1. Electromagnetic proof-mass actuator used in this study.

Figure 2. (a) actual mechanical system, and (b) system for model-free controller design.

Figure 3. Bode plot of T_{xvx1}.

Figure 4. Uncertain plant $\tilde{P}(\mathrm{s})$, which is represented as $P(s)$ with feedback-type fluctuations.

Figure 5. Generalized plant for VCO-based mixed H_2/H_∞ controller design considering parametric uncertainty of the actuator.

Figure 6. Controlled objects: (a) Structure 1, and (b) Structure 2.

Figure 7. Configuration of experimental system: (a) closed-loop system, and (b) experimental setup.

Figure 8. Frequency responses obtained by vibration control experiments with Structure 1: (a) ErC: 0%, ErK: 0%, and (b) ErC: 50%, ErK: −50%.

Figure 9. Frequency responses obtained by vibration control experiments with Structure 2: (a) ErC: 0%, ErK: 0%, and (b) ErC: −50%, ErK: 50%.

Figure 10. Frequency responses obtained by vibration control simulations with Structure 1: (a) ErC: 0%, ErK: 0%, and (b) ErC: 50%, ErK: −50%.

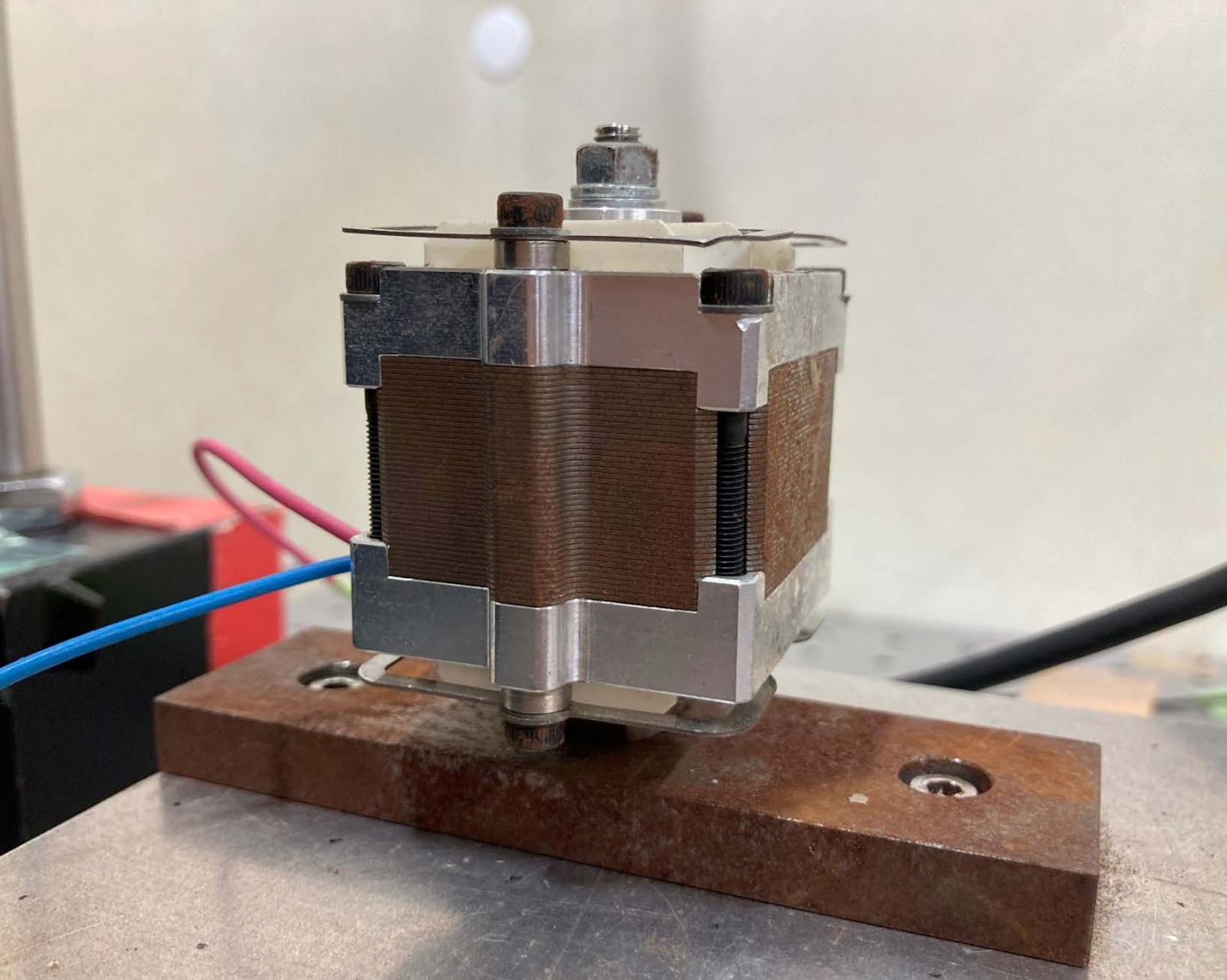

(a)

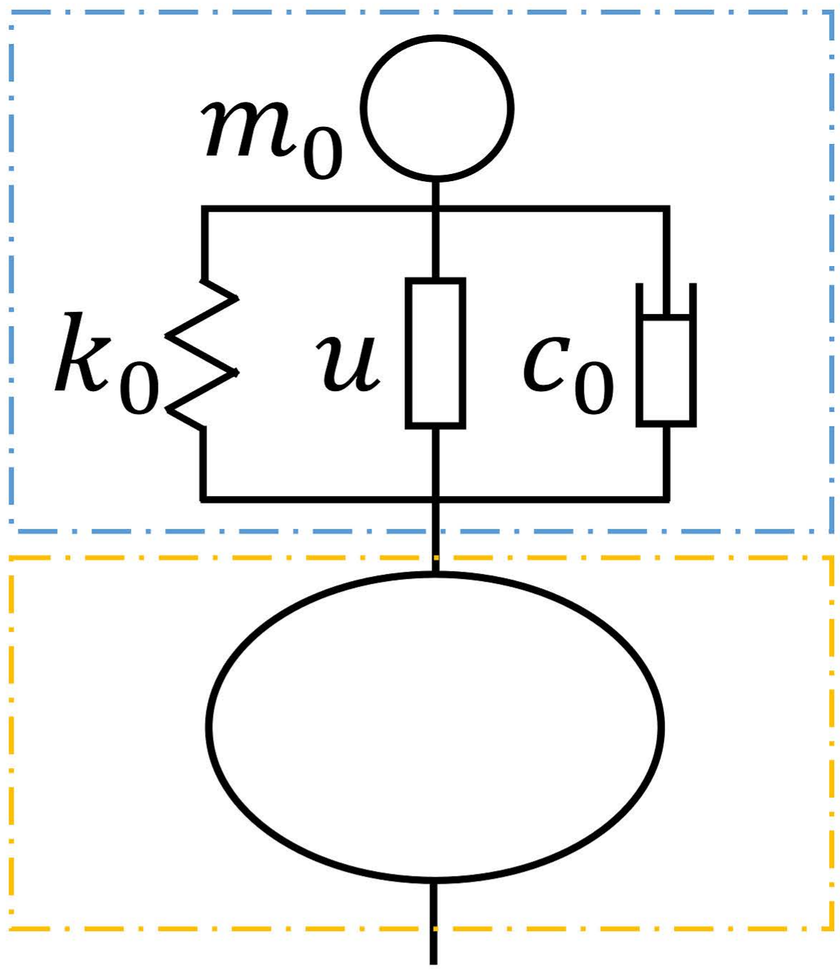

x_0

Actuator

x_1

Actual controlled object

(b)

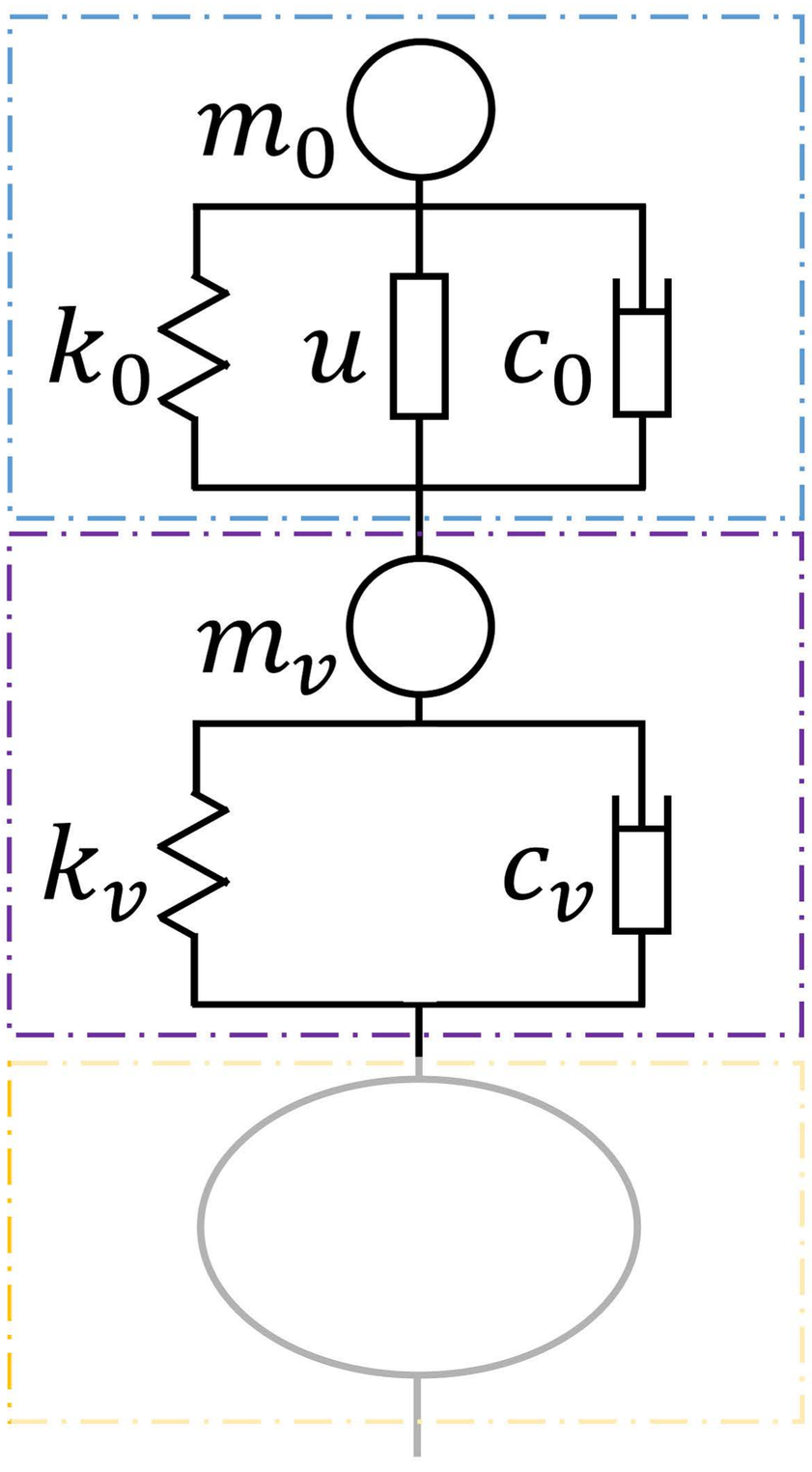

x_0

Actuator

x_v

VCO

x_1

Actual controlled object

Used for controller design

Not used for controller design

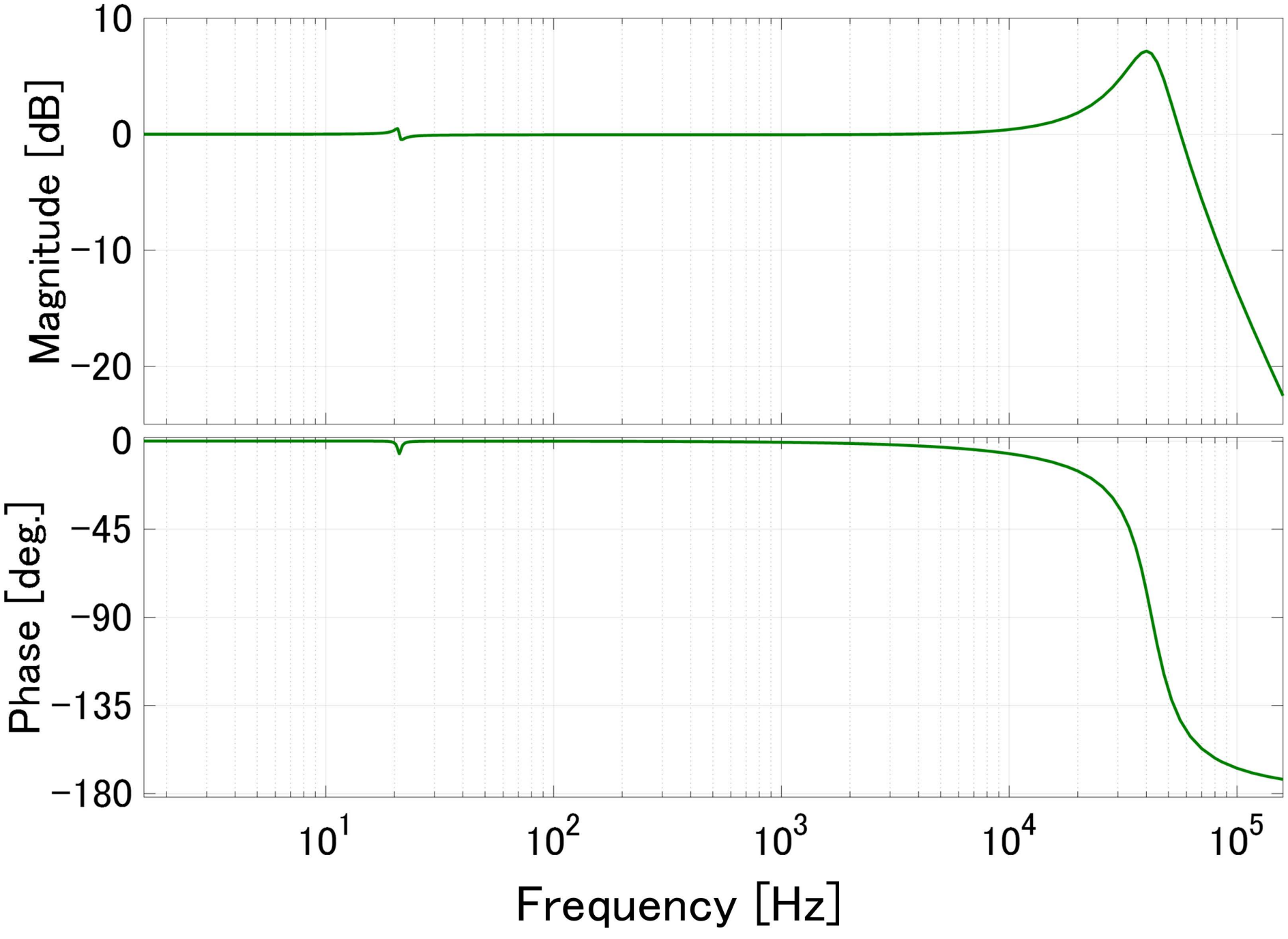
10
0
−10
−20
Magnitude [dB]
0
−45
−90
−135
−180
Phase [deg.]
10^1
10^2
10^3
10^4
10^5
Frequency [Hz]

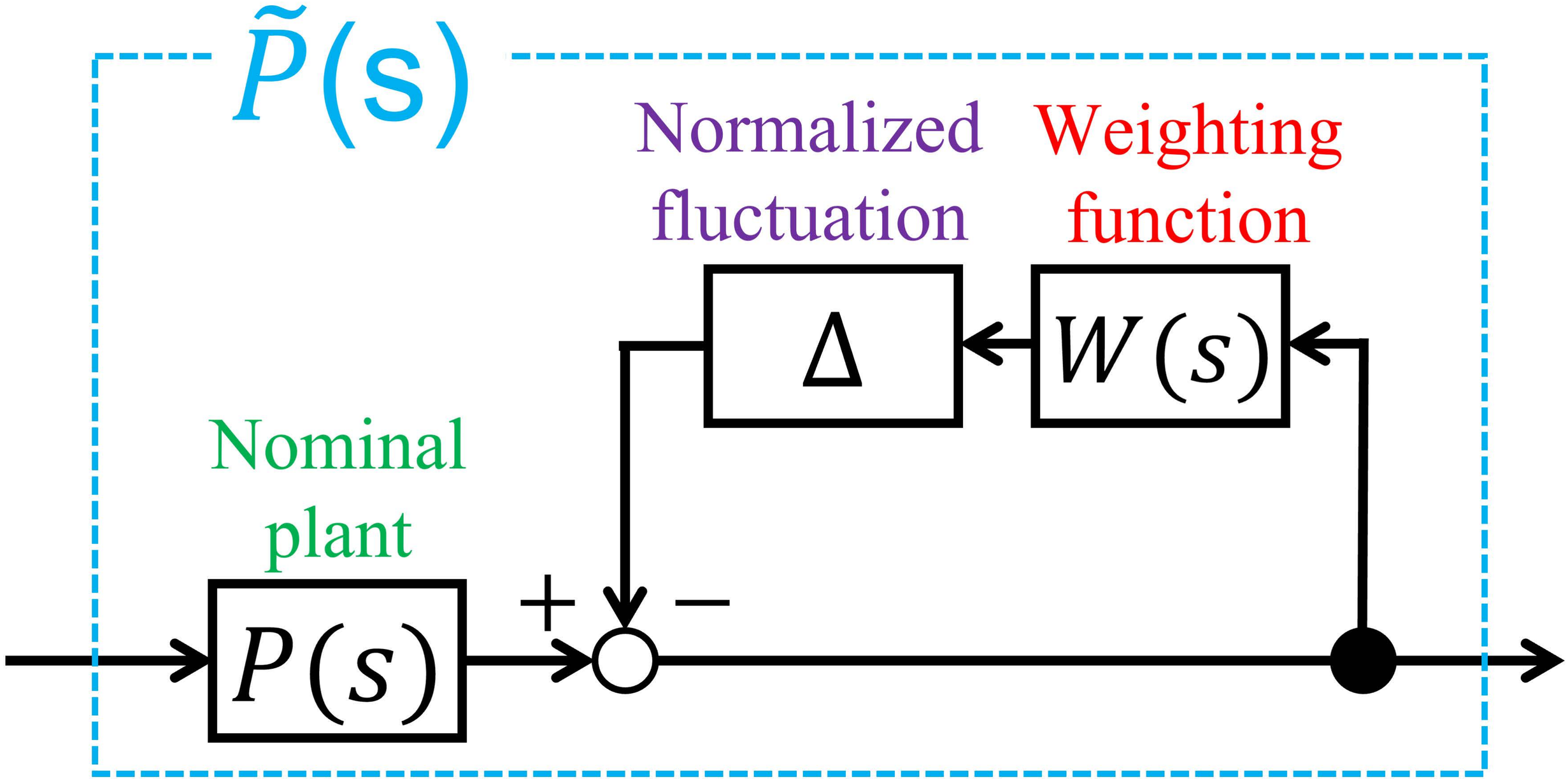
$\tilde{P}(s)$
Normalized fluctuation
Weighting function
Δ
$W(s)$
Nominal plant
$P(s)$
+
−

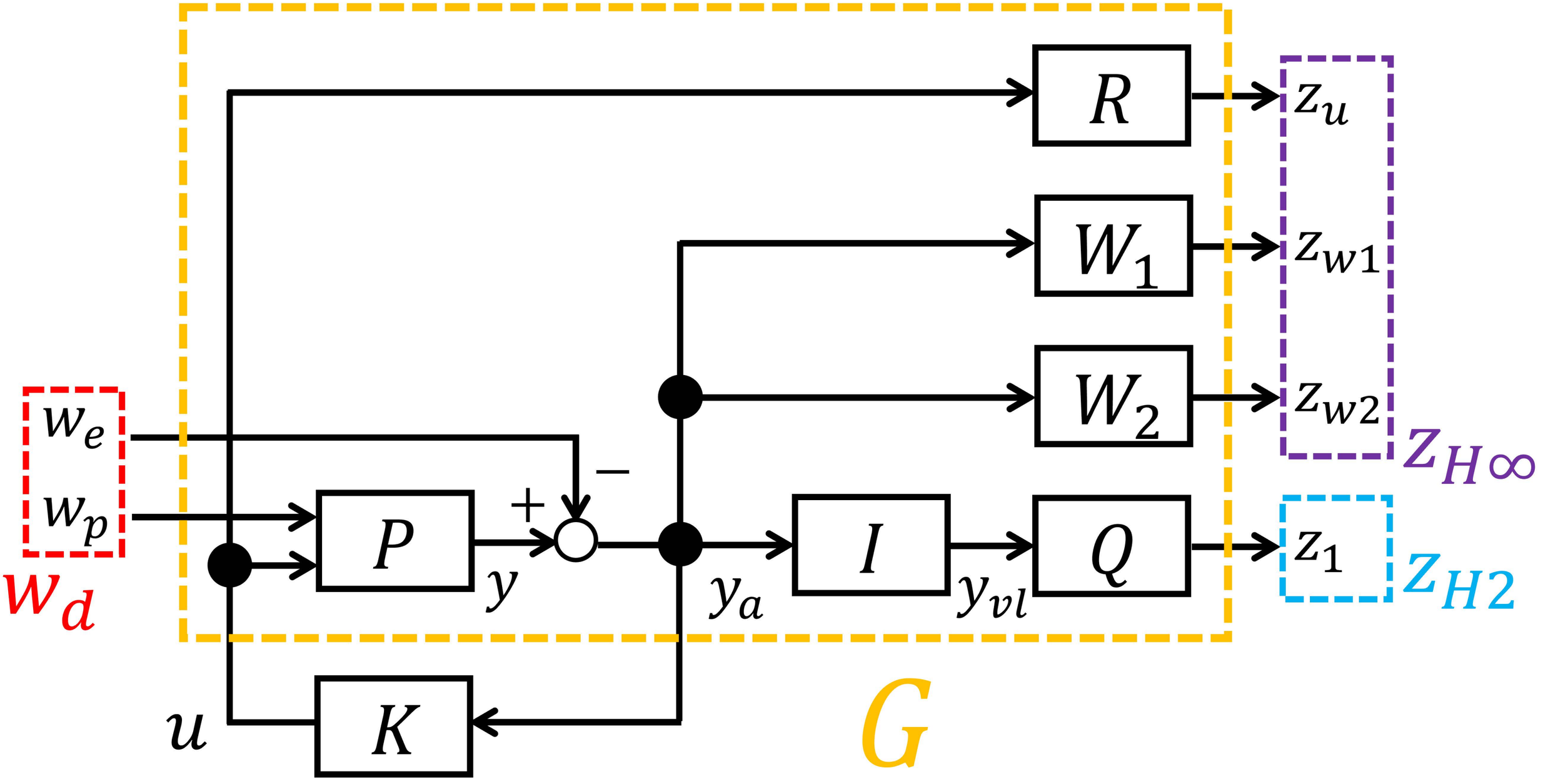
R
W1
W2
Q
I
P
K
we
wp
wd
u
y
ya
yvl
+
−
zu
zw1
zw2
z1
zH∞
zH2
G

(a)

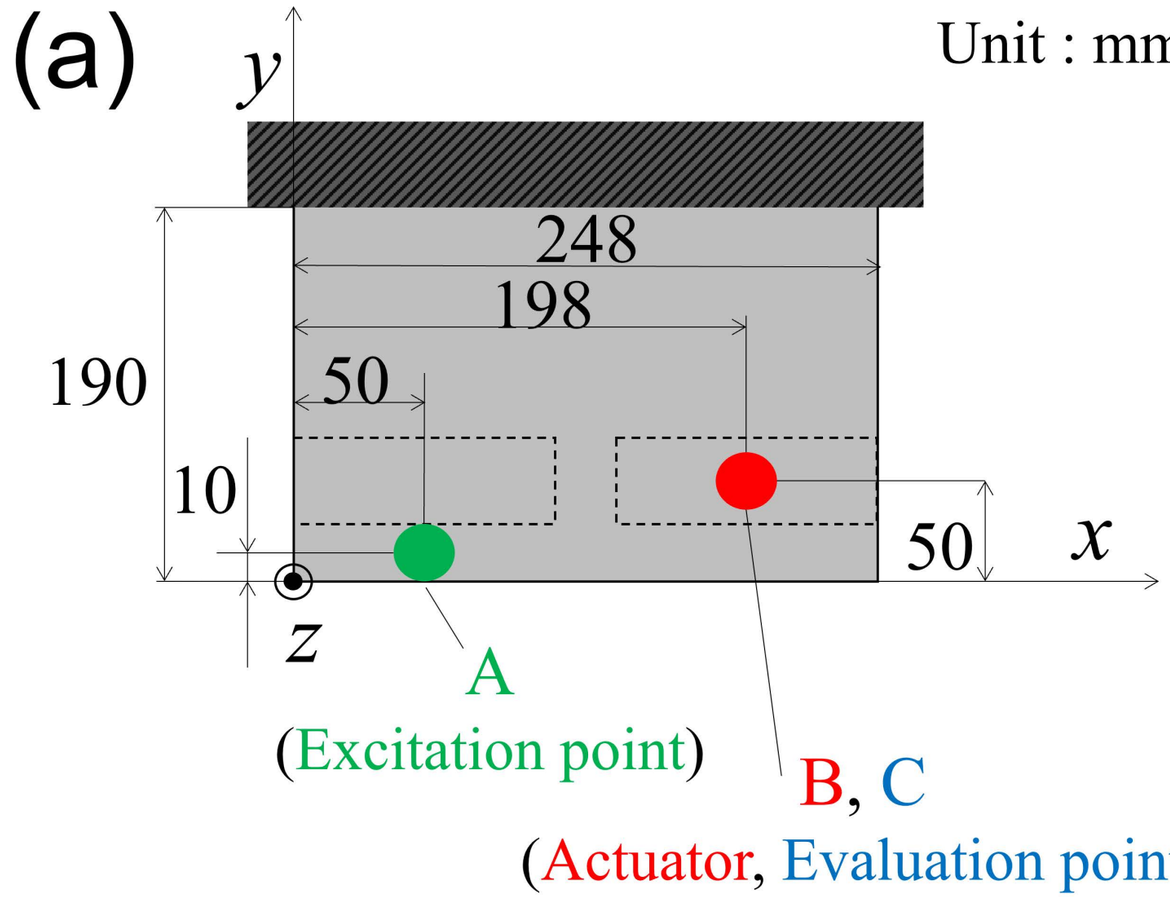
Unit : mm
y
248
198
190
50
10
50
x
z
A
(Excitation point)
B, C
(Actuator, Evaluation point)

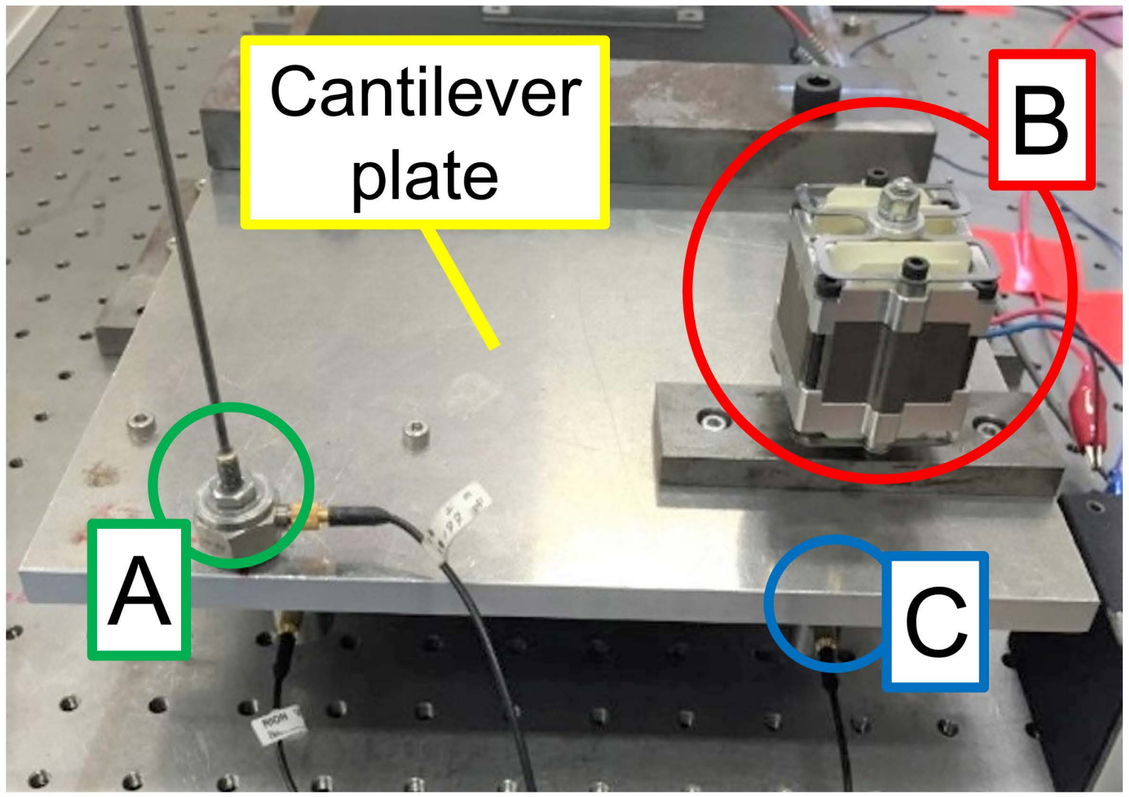
Cantilever plate
B
A
C

(b)

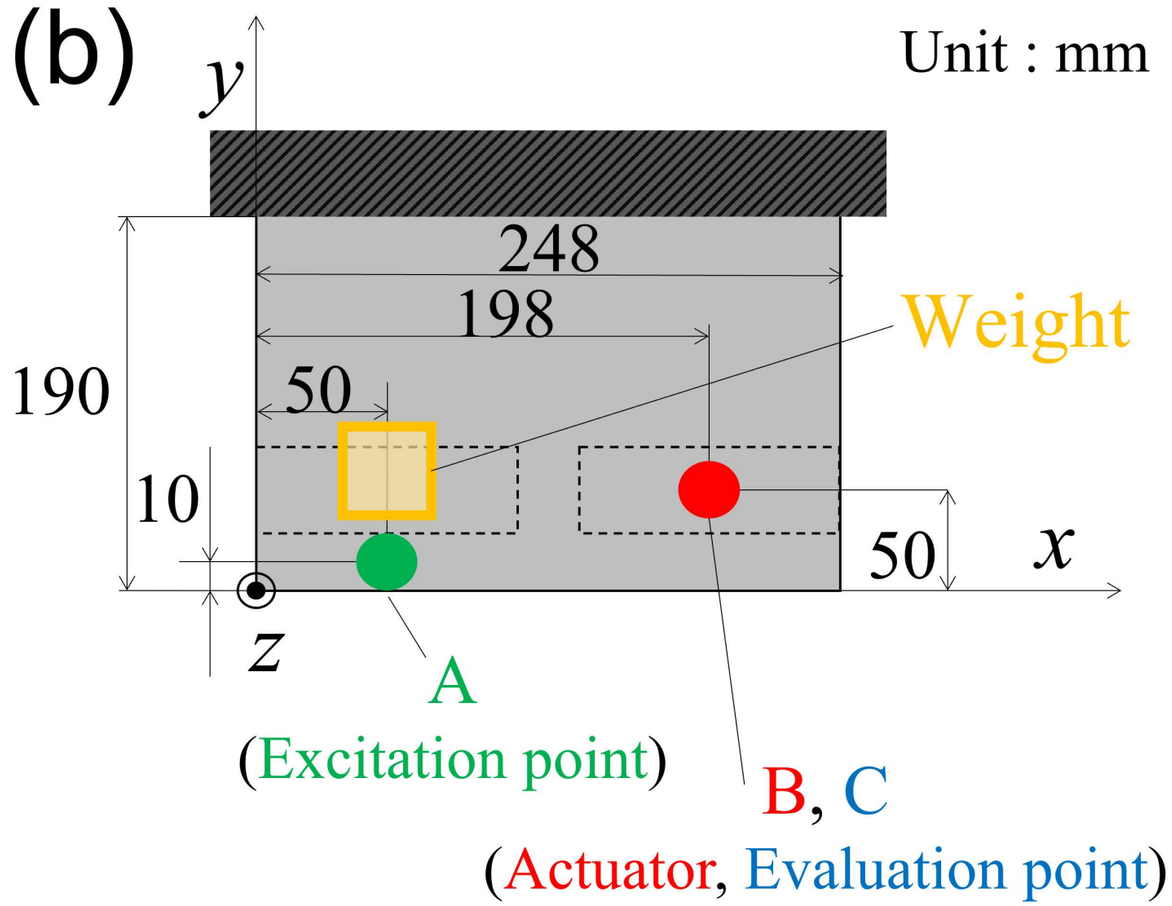
Unit : mm
y
248
198
190
50
10
50
x
Weight
z
A
(Excitation point)
B, C
(Actuator, Evaluation point)

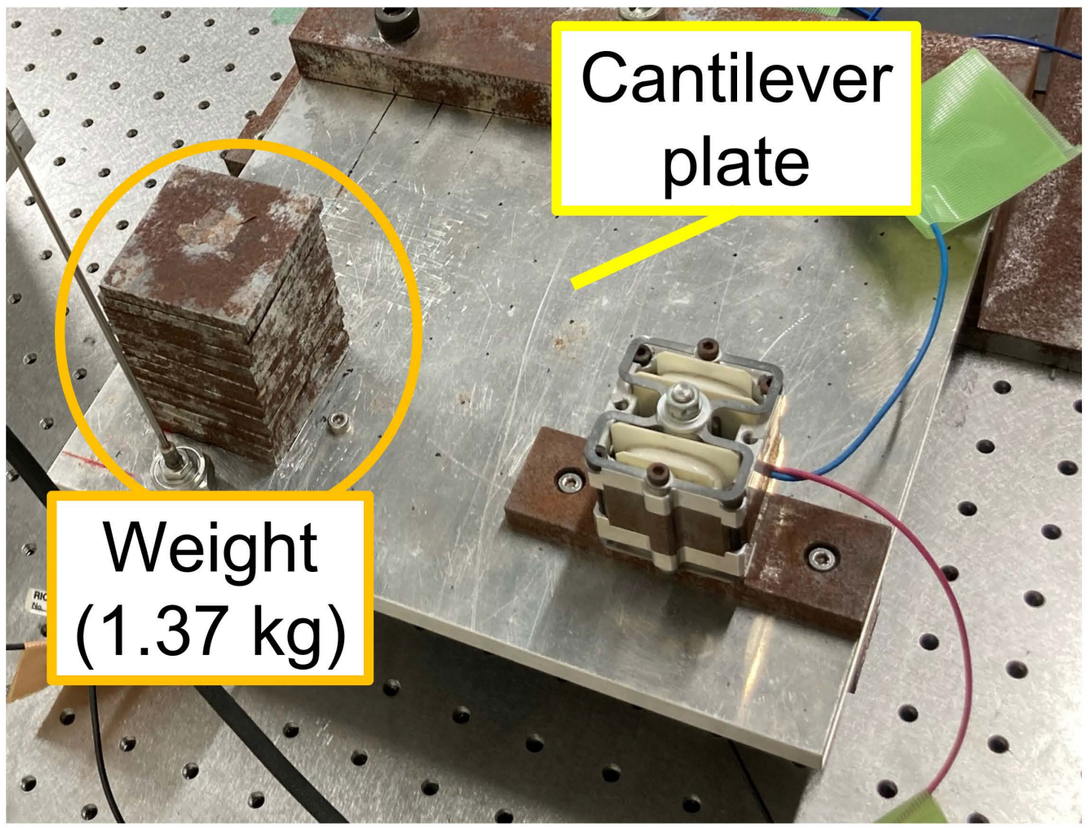
Cantilever plate
Weight (1.37 kg)

(a)

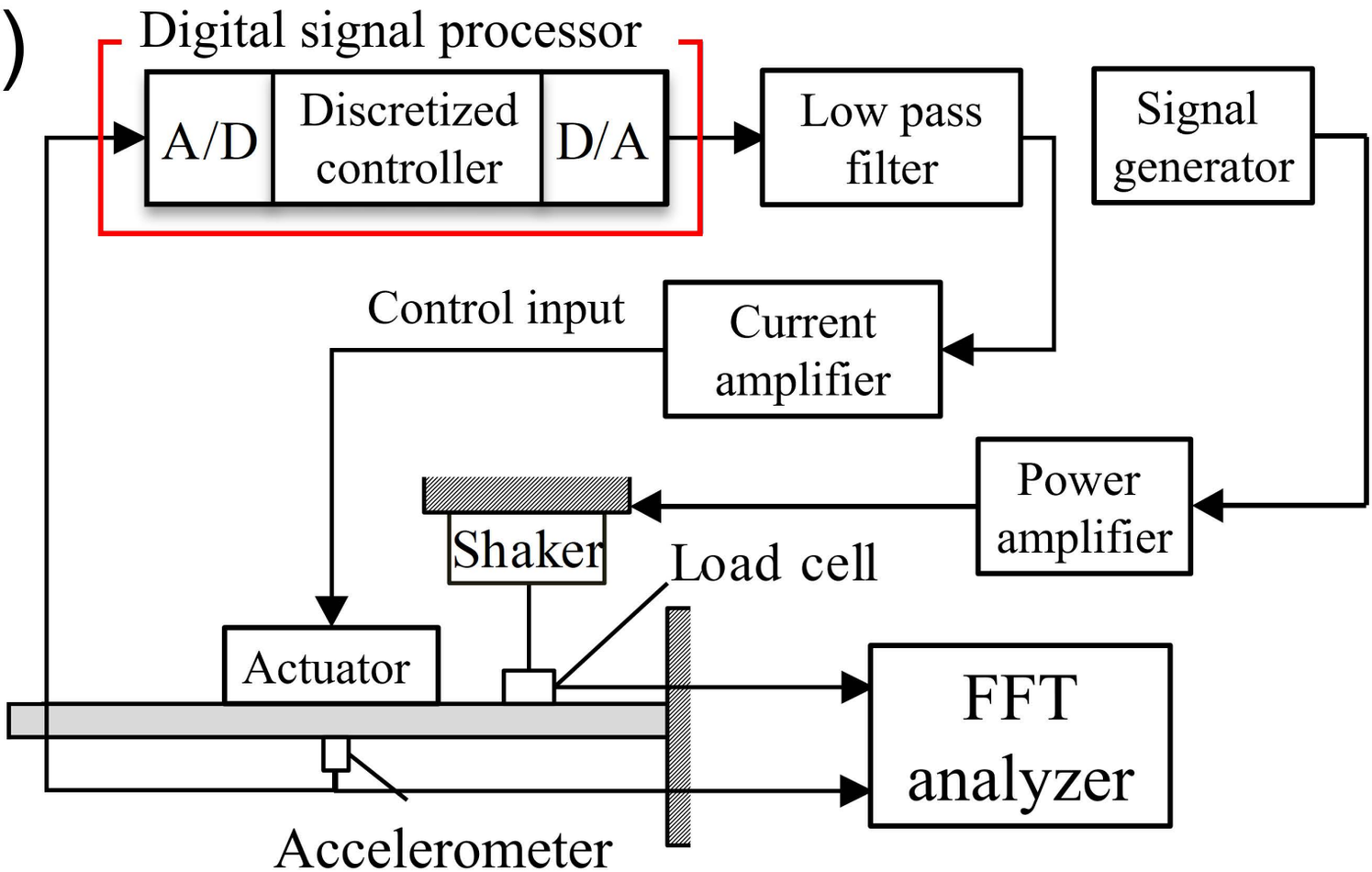
Digital signal processor
A/D
Discretized controller
D/A
Low pass filter
Signal generator
Control input
Current amplifier
Power amplifier
Shaker
Load cell
Actuator
FFT analyzer
Accelerometer

(b)

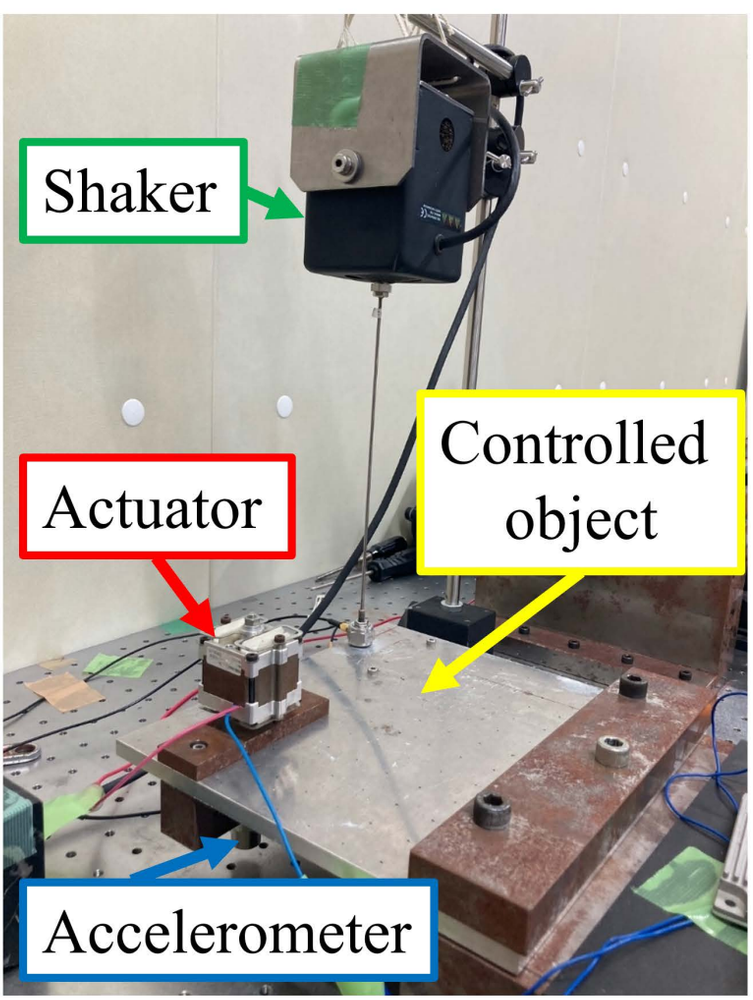
Shaker
Controlled object
Actuator
Accelerometer

(a)

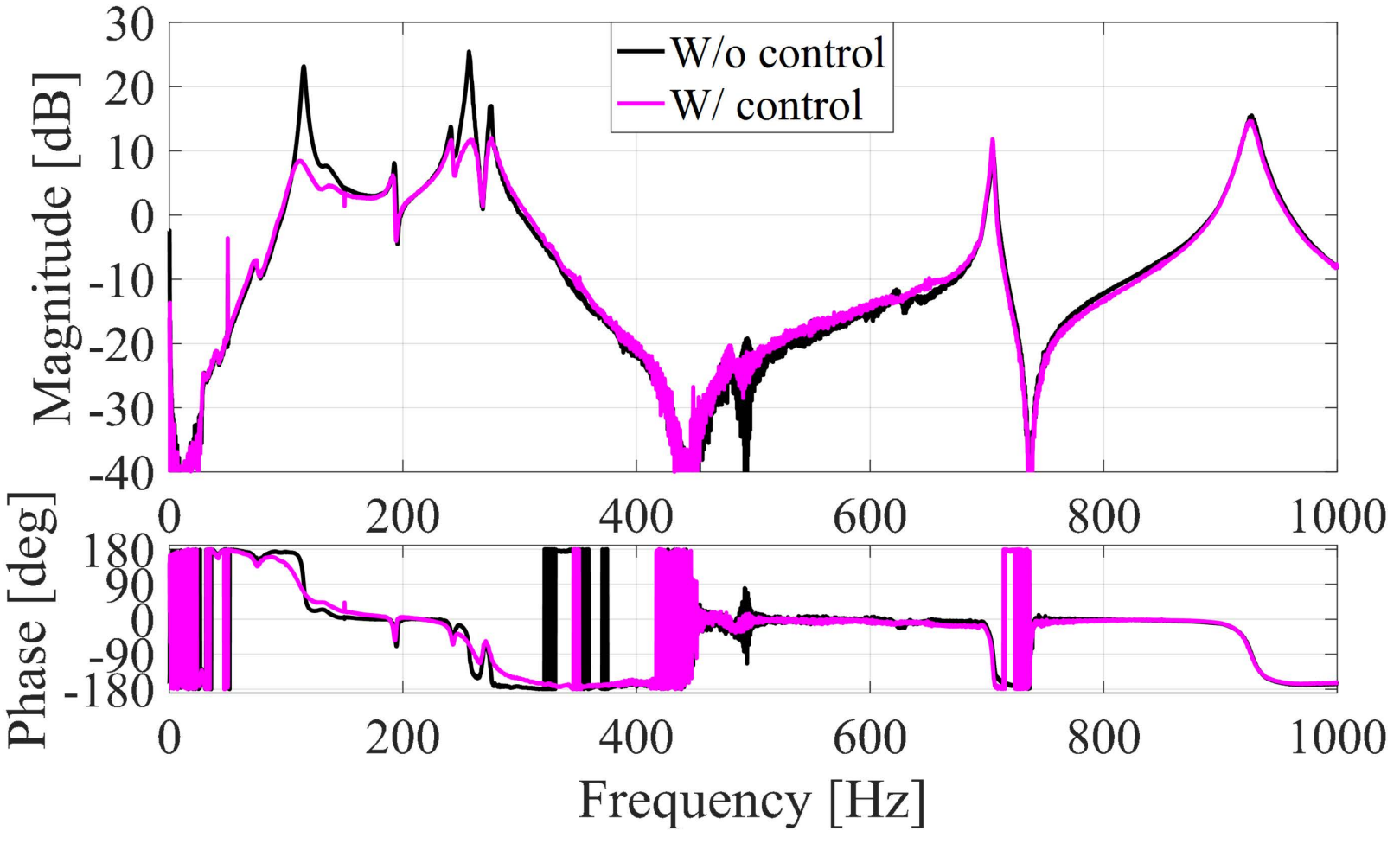
W/o control
W/ control
Magnitude [dB]
30
20
10
0
-10
-20
-30
-40
0
200
400
600
800
1000
Phase [deg]
180
90
0
-90
-180
Frequency [Hz]

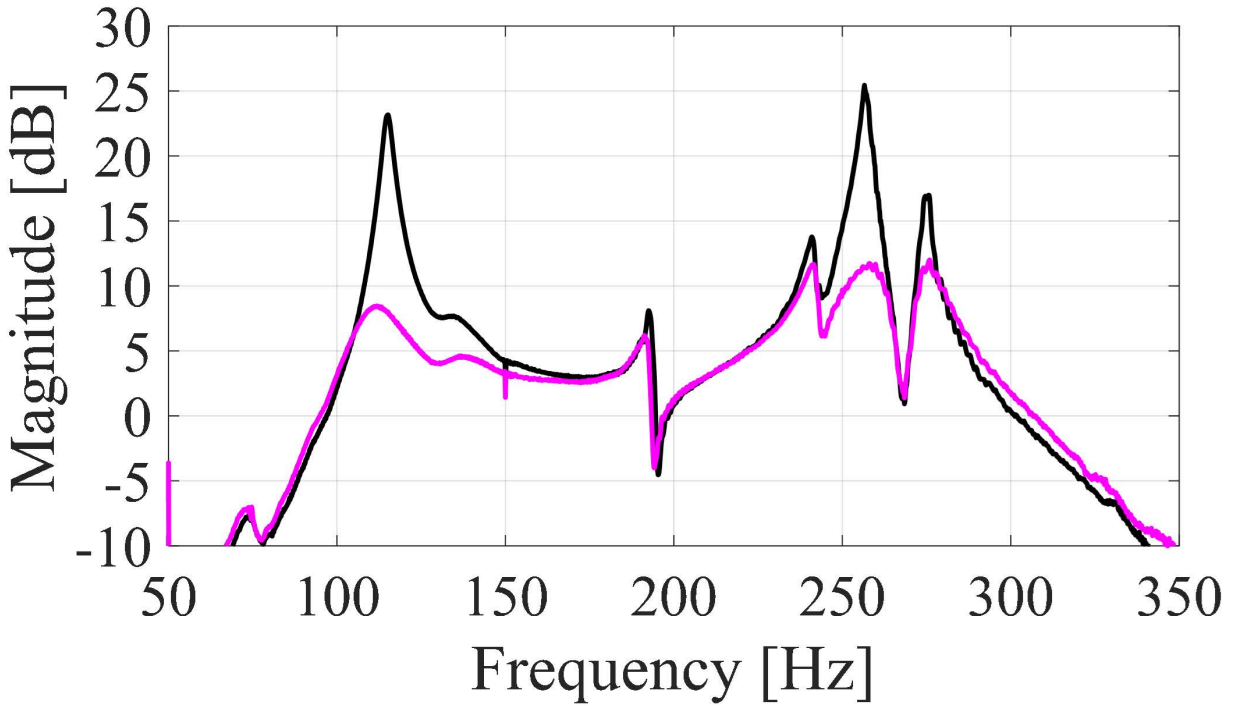
Magnitude [dB]
30
25
20
15
10
5
0
-5
-10
50
100
150
200
250
300
350
Frequency [Hz]

(b)

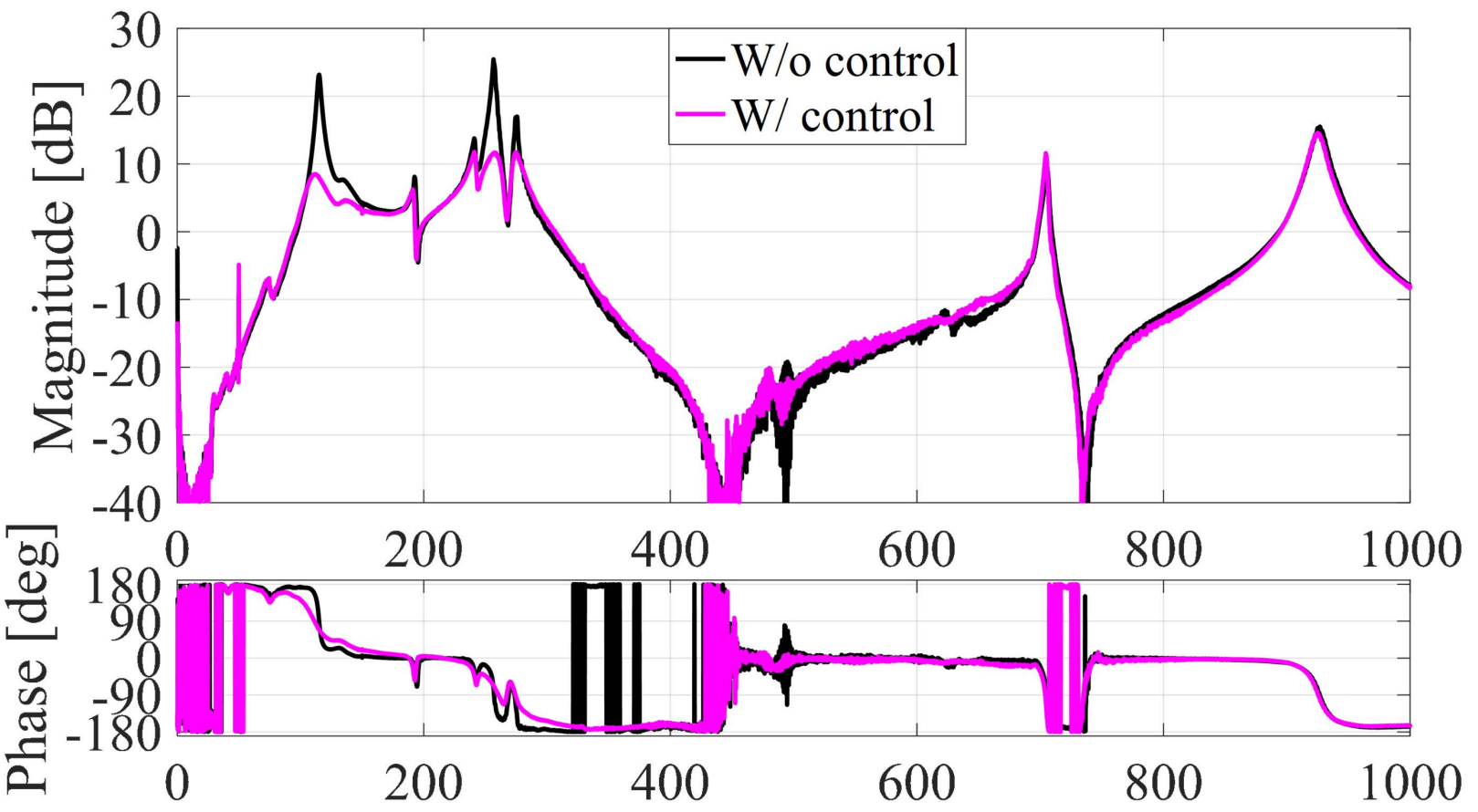
W/o control
W/ control
Magnitude [dB]
30
20
10
0
-10
-20
-30
-40
0
200
400
600
800
1000
Phase [deg]
180
90
0
-90
-180
Frequency [Hz]

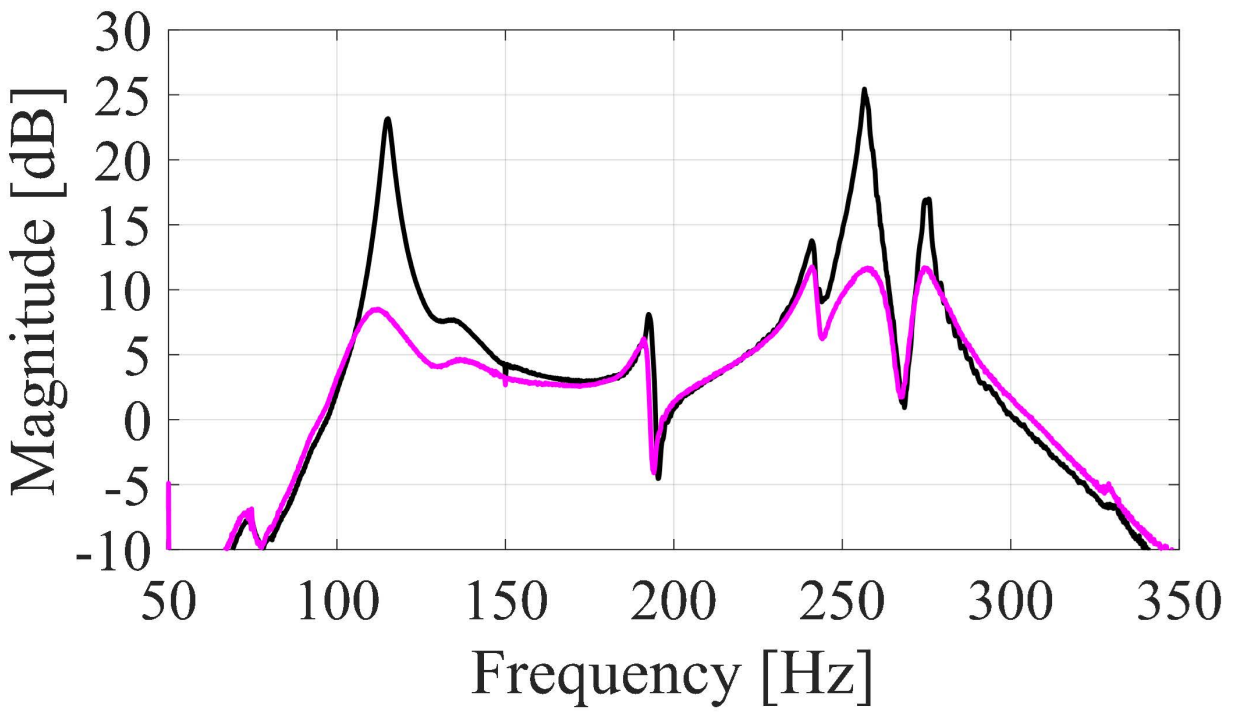
Magnitude [dB]
30
25
20
15
10
5
0
-5
-10
50
100
150
200
250
300
350
Frequency [Hz]

(a)

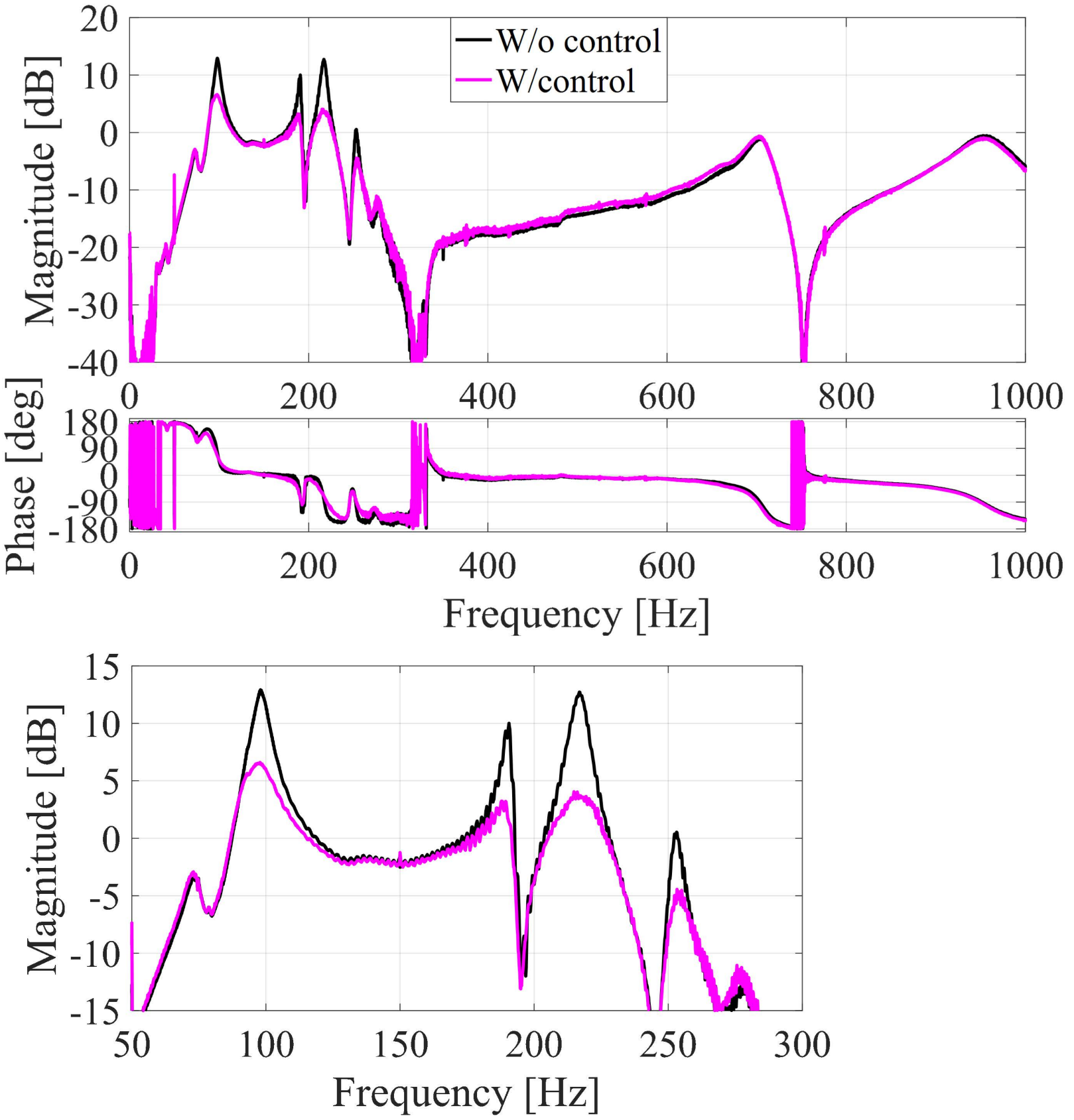
W/o control
W/control
Magnitude [dB]
Phase [deg]
Frequency [Hz]

Magnitude [dB]
Frequency [Hz]

(b)

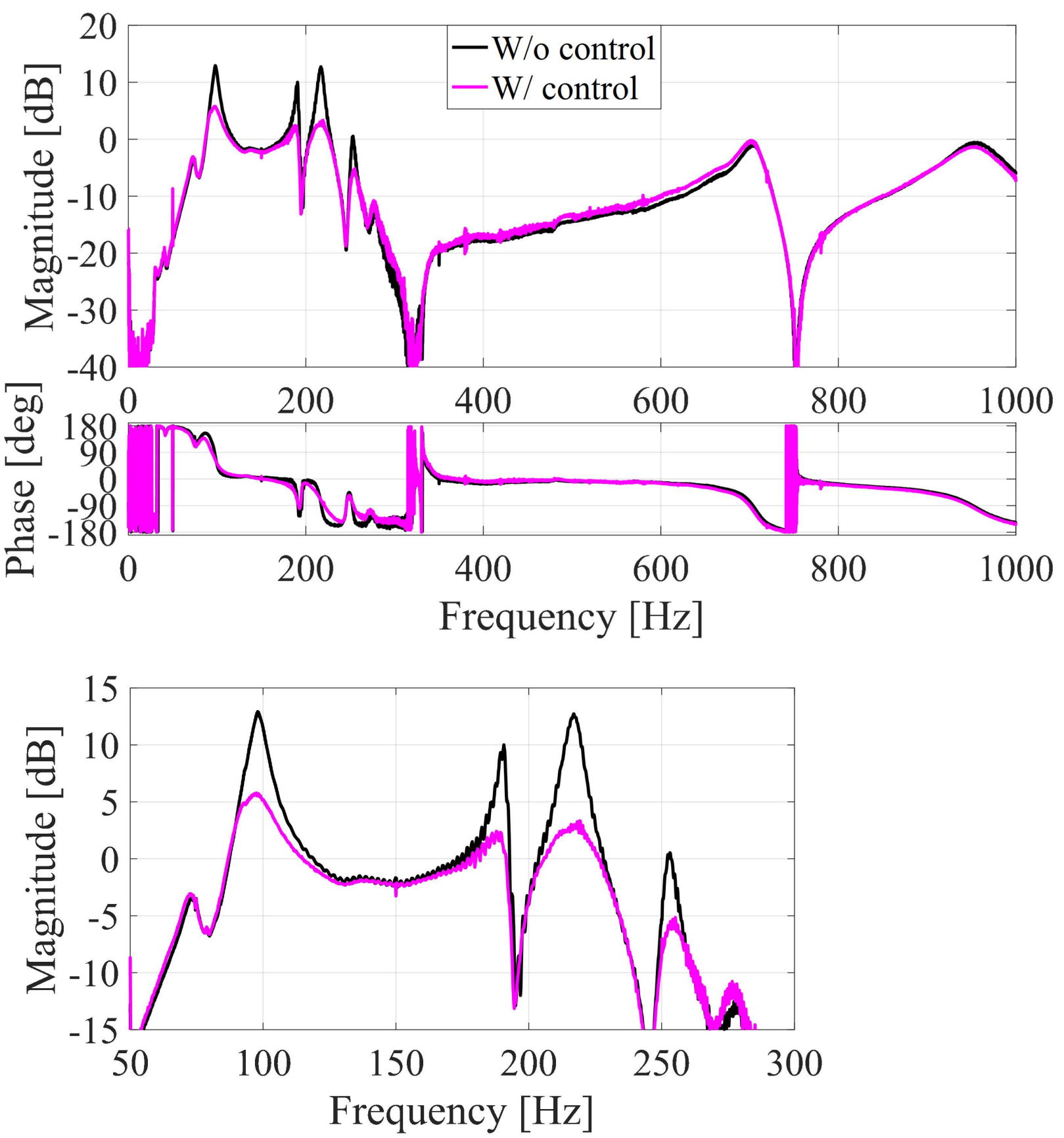
W/o control
W/ control
Magnitude [dB]
Phase [deg]
Frequency [Hz]

Magnitude [dB]
Frequency [Hz]

(a)

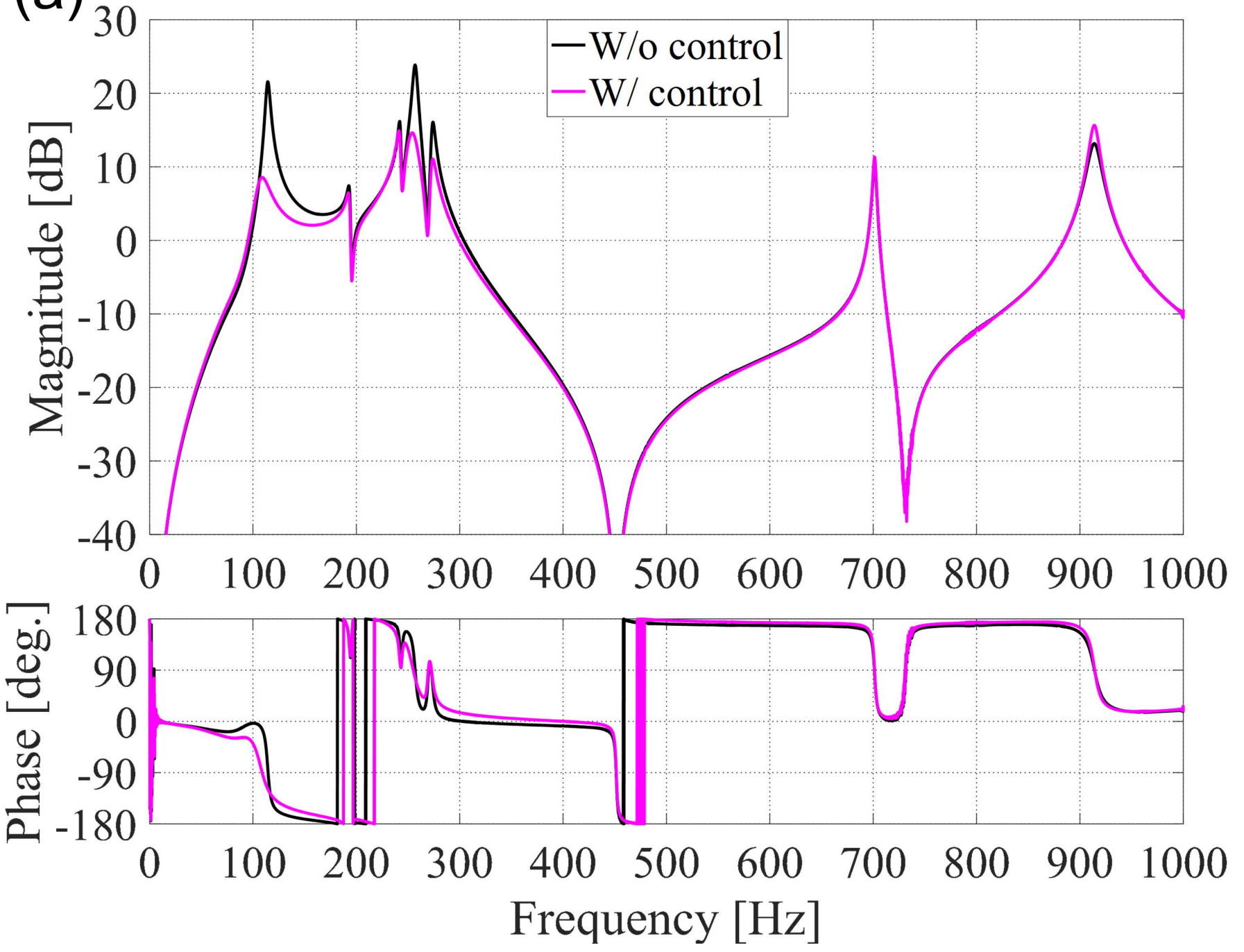
W/o control
W/ control
Magnitude [dB]
30
20
10
0
-10
-20
-30
-40
0
100
200
300
400
500
600
700
800
900
1000
Phase [deg.]
180
90
0
-90
-180
Frequency [Hz]

(b)

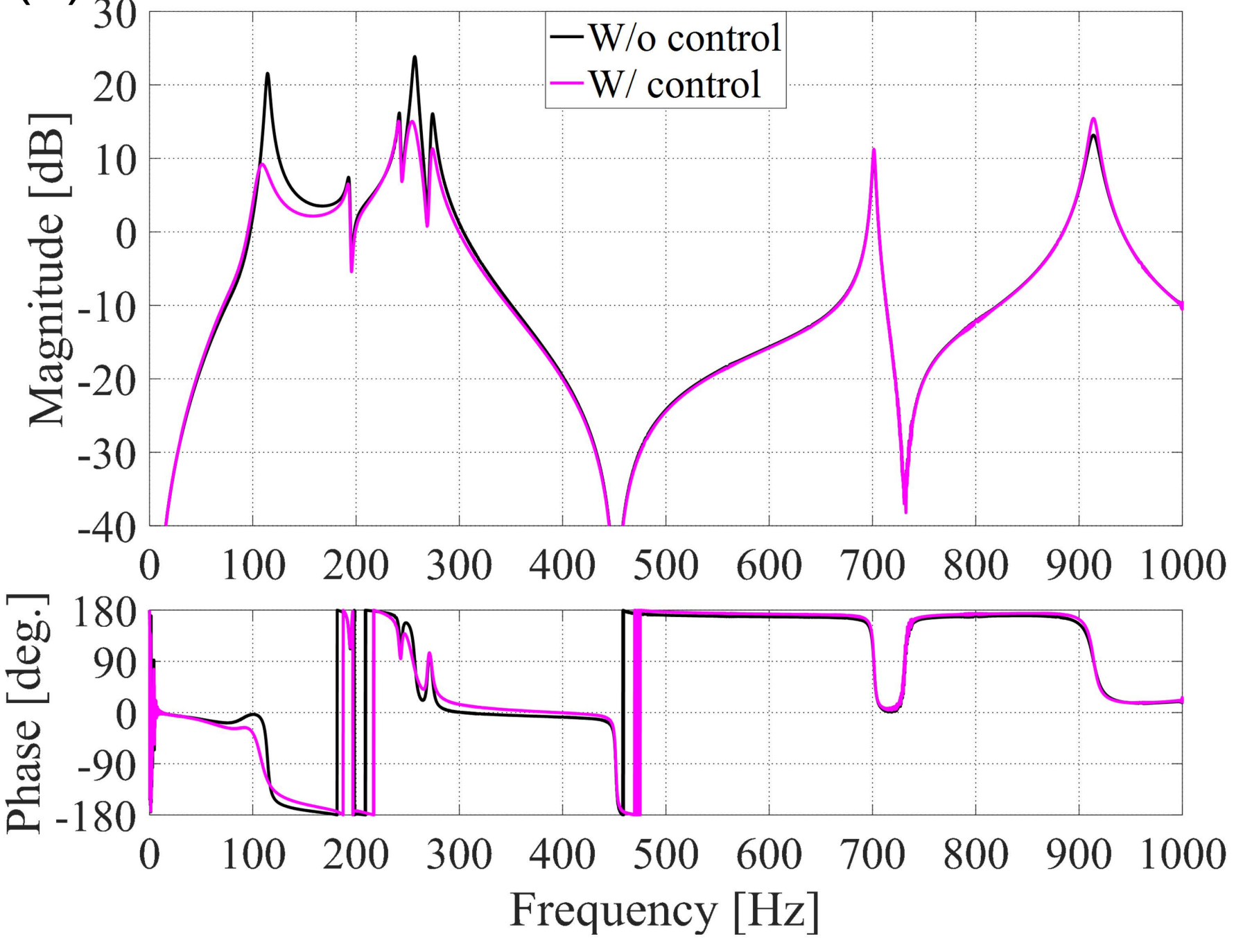
W/o control
W/ control
Magnitude [dB]
30
20
10
0
-10
-20
-30
-40
0
100
200
300
400
500
600
700
800
900
1000
Phase [deg.]
180
90
0
-90
-180
Frequency [Hz]